Synthesis, Structure, and Magnetic Property of a New Open-Framework Manganese Borophosphate, $[NH_4]_4[Mn_9B_2(OH)_2(HPO_4)_4(PO_4)_6]$

Miao Yang, Jihong Yu,* Lei Shi, Peng Chen, Guanghua Li, Yan Chen, and Ruren Xu

State Key Laboratory of Inorganic Synthesis and Preparative Chemistry, College of Chemistry, Jilin University, Changchun 130012, P.R. China

Song Gao

State Key Laboratory of Rare Earth Materials Chemistry and Applications, College of Chemistry and Molecular Engineering, Peking University, Beijing 100871, P.R. China

Received September 28, 2005. Revised Manuscript Received October 26, 2005

A new three-dimensional (3-D) manganese(II) borophosphate, $[NH_4]_4[Mn_9B_2(OH)_2(HPO_4)_4(PO_4)_6]$ (denoted MnBPO-CJ26), has been synthesized by a hydrothermal method. The structure has been determined by single-crystal X-ray diffraction. It crystallizes in the monoclinic space group *C*2/*c* (No. 15) with $a = 32.603(7)$ Å, $b = 10.617(2)$ Å, $c = 10.718(2)$ Å, and $\beta = 108.26(3)°$. Its structure features anionic manganese-phosphate layers $[Mn_9(OH)_2(HPO_4)_4(PO_4)_6]^{10-}$, which are made up from MnO_5, MnO_6, PO_4, and HPO_4 polyhedral units. These anionic layers, parallel to the *bc* plane, are further connected by BO_4 tetrahedra through vertex oxygen atoms forming a novel open framework with 2-D eight-membered ring (8-MR) channels along the [010] and [001] directions. Charge neutrality is achieved by protonated NH_3 molecules. The structure has unique B/P and Mn/P ratios (B/P = 1/5, Mn/P = 9/10). Magnetic measurements indicate that Curie−Weiss behavior above 100 K with $C = 4.404(3)$ cm^3 mol^{-1} K and $\theta = -51.2(5)$ K. The value of C is consistent with an $S = {}^5/_2$ ion with $g \sim 2.0$ (4.38 cm^3 mol^{-1} K). However, the magnetic data reveal a spontaneous magnetization at 8.0 K, indicating a canting of Mn^{2+} moments in the antiferromagnetic ground state.

Introduction

Open-framework metal phosphates have been widely studied for their applications in sorption, separation, and heterogeneous catalysis.[1−3]Recently, metal borophosphate compounds have received much attention because of their fascinating structural architectures and potential applications in catalytic and optical aspects.[4−7] In addition, several borophosphate compounds have been used as antioxidants and fire proofing agents.[8] Since the report of the first zeolite-like metal borophsophate $(C_2H_{10}N_2)[CoB_2P_3O_{12}(OH)]$ in 1996,[9] a number of open-framework borophosphates have been prepared under hydrothermal conditions.[10−15] The structures of borophosphates feature various anionic partial structures, including oligomeric units, chains, ribbons, layers, and 3-D open frameworks.[6] Examples are known as $Co_5[BP_3O_{14}]$,[16] $K_3[B_5PO_{10}(OH)_3]$,[17] $M^IM^{II}(H_2O)_2[BP_2O_8]\cdot H_2O$ (M^I = Na, K, and M^{II} = Mg, Mn, Fe, Co, Ni, Zn),[18] $M^{II}(C_2H_{10}N_2)[B_2P_3O_{12}(OH)]$ (M^{II} = Mg, Mn, Fe, Ni, Cu, Zn),[19] and $M[B_2P_2O_8(OH)]$ (M = Rb, Cs)][20] etc. Their B/P ratios include 1/3, 1/2, 2/3, 1/1, 3/1, and 5/1.[6]

It is noted that the reports on manganese borophosphate materials are rare even though they may exhibit interesting magnetic, spectroscopic, and catalytic properties. Up to now, only two natural seamanites, $Mn_3(OH)_2[BO(OH)_3](PO_3OH)$[21,22] and $Mn_3(OH)_2[B(OH)_4](PO_4)$,[23] and two synthetic 3-D open-framework manganese borophosphates,

* To whom correspondence should be addressed. E-mail: jihong@mail.jlu.edu.cn.

(1) Cheetham, A. K.; Férey, G.; Loiseau, T. *Angew. Chem., Int. Ed.* **1999**, *38*, 3268, and references therein.
(2) Thomas, J. M.; Raja, R.; Sankar, G.; Bell, R. G. *Acc. Chem. Res.* **2001**, *34*, 191.
(3) Yu, J.; Xu, R. *Acc. Chem. Res.* **2003**, *36*, 481, and references therein.
(4) Ahmed, K.; Geisert, C. *J. Vac. Sci Technol. A* **1992**, *10*, 313.
(5) Kniep, R.; Gözel, G.; Eisenmann, B.; Röhr, C.; Asbrand, M.; Kizilyalli, M. *Angew. Chem., Int. Ed. Engl.* **1994**, *33*, 749.
(6) Kniep, R.; Engelhardt, H.; Hauf, C. *Chem. Mater.* **1998**, *10*, 2930, and references therein.
(7) Pan, S.; Wu, Y.; Fu, P.; Zhang, G.; Li, Z.; Du, C.; Chen, C. *Chem. Mater.* **2003**, *15*, 2218.
(8) Geotzman, K.; Karlheionz, D.; Hans-Dieter, N.; Talf, G. Patent CA, C09K015, 1996.
(9) Sevov, S. C. *Angew. Chem., Int. Ed. Engl.* **1996**, *35*, 2630.
(10) Kniep, R.; Schäfer, G.; Engelhardt, H.; Boy, I. *Angew. Chem., Int. Ed.* **1999**, *38*, 3642.
(11) Yilmaz, A.; Bu, X.; Kizilyalli, M.; Stucky, G. D. *Chem. Mater.* **2000,** *12*, 3243.
(12) Yang, G.; Sevov, S. C. *Inorg. Chem.* **2001**, *40*, 2214.
(13) Hang, Y.; Schäfer, G.; Carrillo-Cabrera, W.; Borrmann, H.; Gil, R. C.; Kniep, R. *Chem. Mater.* **2003**, *15*, 4930.
(14) Liu, W.; Ge, M.; Yang, X.; Chen, H.; Li, M.; Zhao, J. *Inorg. Chem.* **2004**, *43*, 3910.
(15) Li, M.; Liu, W.; Ge, M.; Chen, H.; Yang, X.; Zhao, J. *Chem. Commun.* **2004**, 1272.
(16) Bontchev, R. P.; Sevov, S. C. *Inorg. Chem.* **1996**, *35*, 6910.
(17) Hauf, C.; Kniep, R. *Z. Kristallogr.* **1996**, *211*, 707.
(18) Kniep, R.; Will, H. G.; Boy, I.; Röhr, C. *Angew. Chem., Int. Ed. Engl.* **1997**, *36*, 1013.
(19) Kniep, R.; Schäfer, G. *Z. Anorg. Allg. Chem.* **2000**, *626*, 141.
(20) Hauf, C.; Kniep, R. *Z. Naturforsch.* **1997**, *52b*, 1432.
(21) ICSD: Kurkutova, E. N.; Rau, V. G.; Rumanova, I. M. *Dokl. Akad. Nauk SSSR* **1971**, *197*, 1070.

10.1021/cm052170m CCC: $33.50
Published on Web 12/14/2005

$M^IMn(H_2O)_2[BP_2O_8]\cdot H_2O$ (M^I = Na, K)[18] and $Mn(C_2H_{10}N_2)[B_2P_3O_{12}(OH)]$,[19] have been known. The two seamanites have similar 1-D cationic manganese-phosphate chains $[Mn_3(OH)_2(PO_3OH)]^{2+}$ and $[Mn_3(OH)_2(PO_4)]^+$, which are further connected by BO_4 groups forming 3-D open frameworks. All the manganese atoms adopt octahedral coordination. Manganese borophosphate $M^IMn(H_2O)_2[BP_2O_8]\cdot H_2O$ (M^I = Na, K)[18] contains helical ribbons of corner-linked borate and phosphate tetrahedra which are further connected by $MnO_4(H_2O)_2$ octahedra through common vertex oxygen atoms resulting in a 3-D chiral octahedral-tetrahedral framework related to zeolite CZP topology. $Mn(C_2H_{10}N_2)[B_2P_3O_{12}(OH)]$[19] is an analogue of $Co(C_2H_{10}N_2)[B_2P_3O_{12}(OH)]$.[9] It is composed of anionic borophosphate layers made up from tetrahedral BO_4 and PO_4 units forming three- and nine-membered rings. The distorted MnO_6 octahedra pillar the layers, giving rise to an open framework with 1-D 8-MR channels.

Herein, we describe the third synthetic manganese borophosphate $(NH_4)_4Mn_9B_2(OH)_2(HPO_4)_4(PO_4)_6$, designated MnBPO-CJ26 (CJ26: China Jilin University, number 26), with unique B/P and Mn/P ratios (B/P = 1/5, Mn/P = 9/10). Its framework consists of anionic manganese-phosphate layers, $[Mn_9(OH)_2(HPO_4)_4(PO_4)_6]^{10-}$, which are pillared by BO_4 groups forming a 3-D open framework with 2-D 8-MR channels. Magnetic studies reveal that MnBPO-CJ26 displays a canted antiferromagnetic behavior below 8.0 K.

Experimental Section

Synthesis and Characterization. MnBPO-CJ26 was prepared by a hydrothermal method. Typically, a reaction mixture of $Mn(OAc)_2\cdot 4H_2O$ (1 mmol), H_3BO_3 (16.2 mmol), $(NH_4)_2HPO_4$ (3.2 mmol), and H_2O (55.6 mmol) was loaded into a 15 mL Teflon-lined stainless steel autoclave directly and then heated under autogenous pressure at 200 °C for 5 days. The final product containing light pink stick-like crystals was washed with hot water (50 °C) until the residual boric acid was completely removed, and then it was dried in air. X-ray power diffraction (XRD) data were collected on a Rigaku X-ray diffractometer with Cu Kα radiation (λ = 1.5418 Å). Its experimental XRD pattern is in agreement with the simulated one generated on the basis of single-crystal structural data, proving the phase purity of the as-synthesized product (Supporting Information Figure S1). The elemental analysis was conducted on a Perkin-Elemental 2400 elemental analyzer, giving the contents of N and H as 3.61 and 1.28 wt %, respectively (calcd: N, 3.55; H, 1.40 wt %). Inductively coupled plasma (ICP) analysis was performed on a Perkin-Elmer Optima 3300Dv spectrometer and gave the contents of Mn, B, and P as 32.0, 1.54, and 20.1 wt %, respectively (calcd: Mn, 31.4; B, 1.37; P, 19.7 wt %). The infrared (IR) spectrum was recorded within the 400−4000 cm^{-1} region on a Bruker-IFS 66V/S spectrometer using KBr pellets. As seen in Supporting Information Figure S2, the bands at 3498 and 1684 cm^{-1} can be assigned to the stretching and bending vibrations of O−H groups, while the bands at 3226, 3084, 2848, and 1437 cm^{-1} correspond to the stretching and bending vibrations of N−H groups, confirming the presence of NH_4^+ ions.[24] The bands in the region 1097−586 cm^{-1} can be assigned to the asymmetric stretching and bending vibrations of PO_4, BO_4, and B−O−P groups.[25] Thermogravimetric analysis (TGA) was carried out on a Perkin-Elmer TGA 7 unit in the air with a heating rate of 10 °C/min and showed a major weight loss of 11% occurring at 200−510 °C (Supporting Information Figure S3). It is ascribed to the removal of NH_3 molecules (calcd: 4.31 wt %) and H_2O molecules dehydrated from OH groups (calcd: 5.71 wt %) in the product.

Table 1. Crystal Data and Structure Refinement for MnBPO-CJ26[a]

empirical formula	$H_{22}B_2Mn_9N_4O_{42}P_{10}$	
formula weight	1576.00	
temperature	173(2) K	
wavelength	0.71073 Å	
crystal system, space group	monoclinic, *C*2/*c*	
unit cell dimensions	a = 32.603(7) Å	α = 90.00°
	b = 10.617(2) Å	β = 108.26(3)°
	c = 10.718(2) Å	γ = 90.00°
volume	3523.2(12) $Å^3$	
Z, calculated density	4, 2.971 Mg/m^3	
absorption coefficient	3.718 mm^{-1}	
F(000)	3084	
crystal size	0.25 × 0.1 × 0.08 mm^3	
θ range for data collection	2.99−27.45°	
limiting indices	$-41 \le h \le 42$, $-13 \le k \le 13$, $-13 \le l \le 13$	
reflections collected/ unique	16858/4010 [R(int) = 0.0413]	
completeness to θ = 27.45	99.4%	
refinement method	full-matrix least-squares on F^2	
data/restraints/parameters	4010/12/330	
goodness-of-fit on F^2	1.076	
final R indices [$I > 2\sigma(I)$]	R_1 = 0.0313, wR_2 = 0.0801	
R indices (all data)	R_1 = 0.0374, wR_2 = 0.0835	
extinction coefficient	0.00035(5)	
largest diff. peak and hole	1.607 and −0.675 e $Å^{-3}$	

[a] $R_1 = \Sigma(\Delta F/\Sigma(F_o))$; $wR_2 = (\Sigma[w(F_o^2 - F_c^2)])/\Sigma[w(F_o^2)^2]^{1/2}$, $w = 1/\sigma^2(F_o^2)$.

Single-Crystal X-ray Diffraction. A suitable single crystal with dimensions of 0.25 × 0.10 × 0.08 mm^3 was selected for single-crystal X-ray diffraction analysis. The data were collected on a Rigaku RAXIS-RAPID diffractometer equipped with graphite-monochromated Mo Kα radiation (λ = 0.71073Å) at a temperature of 173 K. Data processing was accomplished with the PROCESS-AUTO processing program. Direct methods were used to solve the structure using the SHELXTL crystallographic software package.[26] The structure was solved in the space group of *C*2/*c*. All framework atoms Mn, P, B, and O could be unambiguously located. The two guest atoms located from the difference Fourier map were suggested to be N atoms in two protonated NH_3 molecules by charge balance, IR, and elemental analysis. The N(1) atom was found to be disordered over two sites with different occupancy: N(1)/N(1)′: 0.8/0.2. The H atoms of N(1) and N(1)′ were not added. The H atoms of the N(2) atoms and the hydroxyl groups were subsequently located from the difference Fourier map. The positions of H(4), H(8), and H(16) atoms attached to O(4), O(8), and O(16) were fixed, and the temperature factors of H(4) and H(8) were fixed to 0.08. The non-hydrogen atoms were refined anisotropically. Structure details and selected bond lengths and angles are listed in Tables 1 and 2, respectively.

ESR and Magnetic Measurements. The ESR spectrum was recorded on a powder sample at X band at room temperature on

(22) ICSD: Kurkutova, E. N.; Rau, V. G.; Rumanova, I. M. *Am. Mineral.* **1941**, *26*, 446.
(23) ICSD: Moore, P. B.; Ghose, S. *Am. Mineral.* **1971**, *56*, 1527.
(24) Huang, Y.; Schäferm, G.; Carrillo-Cabrera, W.; Cardoso, R.; Schnelle, W.; Zhao, J.; Kniep, R. *Chem. Mater.* **2001**, *13*, 4348.
(25) Baykal, A.; Klzilyalli, M. *J. Mater. Sci.* **2000**, *35*, 4621.
(26) *SHELXTL Program*, version 5.1; Siemens Industrial Automation, Inc., 1997.

Table 2. Selective Bond Lengths [Å] and Angles [deg] for MnBPO-CJ26[a]

Mn(1)−O(1)	2.192(2)	Mn(1)−O(6)	2.252(3)
Mn(1)−O(2)	2.107(3)	Mn(1)−O(21)	2.127(2)
Mn(1)−O(5)#1	2.139(2)	Mn(2)−O(5)	2.154(2)
Mn(2)−O(6)	2.145(2)	Mn(2)−O(7)	2.169(3)
Mn(2)−O(9)	2.114(2)	Mn(2)−O(18)	2.172(2)
Mn(2)−O(19)	2.314(2)	Mn(3)−O(9)	2.117(3)
Mn(3)−O(9)#2	2.117(3)	Mn(3)−O(10)	2.226(4)
Mn(3)−O(10)#2	2.226(4)	Mn(3)−O(12)	2.569(3)
Mn(3)−O(12)#2	2.569(3)	Mn(4)−O(11)	2.163(2)
Mn(4)−O(12)	2.063(3)	Mn(4)−O(13)	2.102(3)
Mn(4)−O(14)	2.170(2)	Mn(4)−O(15)#3	2.225(2)
Mn(5)−O(11)	2.267(3)	Mn(5)−O(15)	2.113(2)
Mn(5)−O(16)	2.158(3)	Mn(5)−O(18)	2.209(2)
Mn(5)−O(14)	2.230(2)	Mn(5)−O(19)	2.184(2)
P(1)−O(6)	1.526(3)	P(1)−O(7)#1	1.498(3)
P(1)−O(8)	1.543(2)	P(1)−O(10)#1	1.544(3)
P(2)−O(9)	1.543(2)	P(2)−O(11)	1.541(2)
P(2)−O(12)#2	1.530(3)	P(2)−O(13)#4	1.546(2)
P(3)−O(1)#5	1.515(2)	P(3)−O(15)#3	1.549(2)
P(3)−O(17)	1.551(2)	P(3)−O(18)	1.533(2)
P(4)−O(14)#4	1.547(2)	P(4)−O(19)	1.538(2)
P(4)−O(20)	1.581(3)	P(4)−O(21)	1.513(2)
P(5)−O(2)	1.513(3)	P(5)−O(3)	1.567(2)
P(5)−O(4)	1.545(3)	P(5)−O(5)	1.536(3)
B(1)−O(3) #6	1.469(4)	B(1)−O(16)	1.471(4)
B(1)−O(17)	1.472(4)	B(1)−O(20)#3	1.477(4)
O(2)−Mn(1)−O(21)	90.29(10)	O(2)−Mn(1)−O(5)#1	124.59(10)
O(21)−Mn(1)−O(5)#1	90.65(9)	O(2)−Mn(1)−O(1)	100.23(10)
O(21)−Mn(1)−O(1)	168.30(10)	O(5)#1−Mn(1)−O(1)	87.60(9)
O(2)−Mn(1)−O(6)	106.91(9)	O(21)−Mn(1)−O(6)	87.09(9)
O(5)#1−Mn(1)−O(6)	128.46(9)	O(1)−Mn(1)−O(6)	84.97(9)
O(18)−Mn(2)−O(19)	77.95(8)	O(9)−Mn(2)−O(6)	93.46(10)
O(9)−Mn(2)−O(5)	162.08(10)	O(6)−Mn(2)−O(5)	96.05(10)
O(9)−Mn(2)−O(7)	80.04(15)	O(6)−Mn(2)−O(7)	92.20(11)
O(5)−Mn(2)−O(7)	84.45(14)	O(9)−Mn(2)−O(18)	85.49(9)
O(6)−Mn(2)−O(18)	165.41(9)	O(5)−Mn(2)−O(18)	89.02(9)
O(7)−Mn(2)−O(18)	101.93(11)	O(9)−Mn(2)−O(19)	93.20(9)
O(6)−Mn(2)−O(19)	87.58(9)	O(5)−Mn(2)−O(19)	102.32(9)
O(7)−Mn(2)−O(19)	173.22(14)	O(9)−Mn(3)−O(9)#2	140.91(14)
O(9)−Mn(3)−O(10)#2	85.11(11)	O(9)#2−Mn(3)−O(10)#2	117.12(11)
O(9)−Mn(3)−O(10)	117.12(11)	O(9)#2−Mn(3)−O(10)	85.11(11)
O(10)#2−Mn(3)−O(10)	112.74(16)	O(9)−Mn(3)−O(12)#2	61.27(9)
O(9)#2−Mn(3)−O(12)#2	87.00(9)	O(10)#2−Mn(3)−O(12)#2	86.46(9)
O(10)−Mn(3)−O(12)#2	160.76(10)	O(9)−Mn(3)−O(12)	87.00(9)
O(9)#2−Mn(3)−O(12)	61.27(9)	O(10)#2−Mn(3)−O(12)	160.76(10)
O(10)−Mn(3)−O(12)	86.46(9)	O(12)#2−Mn(3)−O(12)	74.37(11)
O(12)−Mn(4)−O(13)	93.01(10)	O(12)−Mn(4)−O(11)	94.66(10)
O(13)−Mn(4)−O(11)	120.45(9)	O(12)−Mn(4)−O(14)	170.90(10)
O(13)−Mn(4)−O(14)	95.95(10)	O(11)−Mn(4)−O(14)	79.40(9)
O(12)−Mn(4)−O(15)#3	93.30(9)	O(13)−Mn(4)−O(15)#3	109.70(9)
O(11)−Mn(4)−O(15)#3	128.58(9)	O(14)−Mn(4)−O(15)#3	85.21(9)
O(15)−Mn(5)−O(16)	108.78(9)	O(15)−Mn(5)−O(19)	92.67(9)
O(16)−Mn(5)−O(19)	96.48(9)	O(15)−Mn(5)−O(18)	165.83(9)
O(16)−Mn(5)−O(18)	84.24(9)	O(19)−Mn(5)−O(18)	79.99(9)
O(15)−Mn(5)−O(14)	99.22(9)	O(16)−Mn(5)−O(14)	84.57(9)
O(19)−Mn(5)−O(14)	167.06(9)	O(18)−Mn(5)−O(14)	87.30(9)
O(15)−Mn(5)−O(11)	88.49(9)	O(16)−Mn(5)−O(11)	155.92(9)
O(19)−Mn(5)−O(11)	99.41(9)	O(18)−Mn(5)−O(11)	80.86(9)
O(14)−Mn(5)−O(11)	75.96(9)	O(7)#1−P(1)−O(6)	109.93(18)
O(7)#1−P(1)−O(8)	107.34(17)	O(6)−P(1)−O(8)	112.89(14)
O(7)#1−P(1)−O(10)#1	107.5(3)	O(6)−P(1)−O(10)#1	111.50(16)
O(8)−P(1)−O(10)#1	107.43(17)	O(12)#2−P(2)−O(11)	114.05(14)
O(12)#2−P(2)−O(9)	103.86(14)	O(11)−P(2)−O(9)	110.67(14)
O(12)#2−P(2)−O(13)#4	111.63(15)	O(11)−P(2)−O(13)#4	108.07(14)
O(9)−P(2)−O(13)#4	108.42(14)	O(1)#5−P(3)−O(18)	113.45(13)
O(1)#5−P(3)−O(15)#3	111.60(14)	O(18)−P(3)−O(15)#3	106.41(13)
O(1)#5−P(3)−O(17)	107.47(14)	O(18)−P(3)−O(17)	110.61(13)
O(15)#3−P(3)−O(17)	107.16(14)	O(21)−P(4)−O(19)	113.57(13)
O(21)−P(4)−O(14)#4	110.91(13)	O(19)−P(4)−O(14)#4	110.65(13)
O(21)−P(4)−O(20)	106.01(14)	O(19)−P(4)−O(20)	107.91(14)
O(14)#4−P(4)−O(20)	107.45(13)	O(2)−P(5)−O(5)	110.43(15)
O(2)−P(5)−O(4)	112.06(15)	O(5)−P(5)−O(4)	111.01(14)
O(2)−P(5)−O(3)	111.06(14)	O(5)−P(5)−O(3)	104.21(12)
O(4)−P(5)−O(3)	107.80(14)	O(3)#6−B(1)−O(17)	109.8(3)
O(3)#6−B(1)−O(16)	108.0(3)	O(17)−B(1)−O(16)	113.0(3)
O(3)#6−B(1)−O(20)#3	105.9(3)	O(17)−B(1)−O(20)#3	110.9(3)
O(16)−B(1)−O(20)#3	109.0(3)		

[a] Symmetry transformations used to generate equivalent atoms: (#1) x, $-y+2$, $z+{}^1/_2$; (#2) $-x$, y, $-z+{}^1/_2$; (#3) x, $-y+3$, $z-{}^1/_2$; (#4) x, $-y+3$, $z+{}^1/_2$; (#5) x, $-y+2$, $z-{}^1/_2$; (#6) $-x+{}^1/_2$, $-y+{}^5/_2$, $-z+1$.

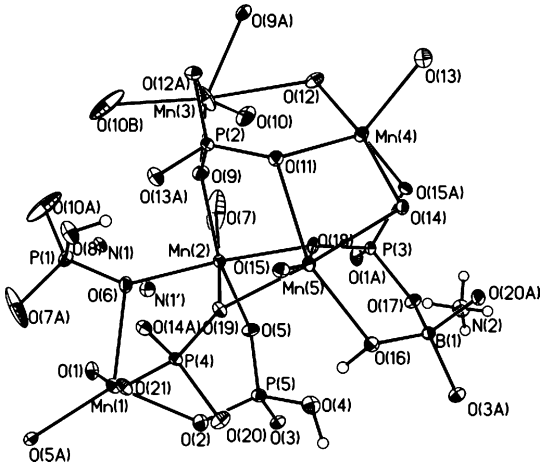

Figure 1. Thermal ellipsoid plot (50% probability) and atomic labeling scheme of MnBPO-CJ26.

an ER 200D ESR spectroscope. The magnetic measurement of a powder sample was performed on a Quantum-Design MPMS-XL SQUID magnetometer. Data were collected over the temperature range from 4 to 300 K, both after cooling in zero applied field (ZFC) and in the measuring field of 20, 100, 1000, and 5000 Oe (FC). Magnetization data were collected at 4 K as a function of applied field in the range from 0 to 50 kOe. Temperature dependence of ac susceptibility was measured in zero applied dc field over the temperature range from 4 to 30 K with ac field frequencies $f = 1$, 11, 111, and 999 Hz and driving amplitude $h = 2$ Oe.

Results and Discussion

Crystal Structure. MnBPO-CJ26 consists of an open framework with macro-anion $[Mn_9B_2(OH)_2(HPO_4)_4(PO_4)_6]^{4-}$. Charge neutrality is achieved by protonated NH_3 molecules. It shows unique B/P and Mn/P ratios (B/P = 1/5, Mn/P = 9/10). To the best of our knowledge, MnBPO-CJ26 possesses the smallest B/P ratio in the family of borophsopahtes. As seen in Figure 1, each asymmetric unit contains five crystallographically distinct Mn sites. Mn(1) and Mn(4) are pentacoordinated to five oxygen atoms (Mn(1)−O_{av}: 2.164 Å; Mn(4)−O_{av}: 2.145Å) to form a trigonal bipyramid, respectively. Although the pentacoordinated manganese atom is common in manganese phosphates, it is first observed in manganese borophosphate materials. Mn(2), Mn(3), and Mn(5) are octahedrally coordinated to six oxygen atoms (Mn(2)−O_{av}: 2.178 Å; Mn(3)−O_{av}: 2.304 Å; Mn(5)−O_{av}: 2.194 Å) to form an octahedron, respectively. The Mn−O bond lengths in MnBPO-CJ26 are comparable to those in the reported manganese borophosphate and manganese phosphate materials.[18,19,27,28] Bond-valence calculations[29] suggest that all the manganese atoms are present as Mn^{2+}, and this is further confirmed by magnetic measurements which will be discussed below. Of the five crystallographically distinct P atoms, P(1) makes one P−μ_3-O−Mn(Mn) bond and two P−O−Mn bonds and possesses a terminal P−O(8)H group; P(2) makes three P−μ_3-O−Mn(Mn) bonds

(27) Escobal, J.; Pizarro, J. L.; Mesa, J. L.; Lezama, L.; Loazcuaga, R.; Arriortua, M. I.; Rojo, T. *Chem. Mater.* **2000**, *12*, 376.
(28) Escobal, J.; Mesa, J. L.; Pizarro, J. L.; Lezama, L.; Loazcuaga, R.; Rojo, T. *J. Mater. Chem.* **1999**, *9*, 2691.
(29) Brese, N. E.; O'Keefe, M. *Acta Crystallogr., Sect. B* **1991**, *47*, 192.

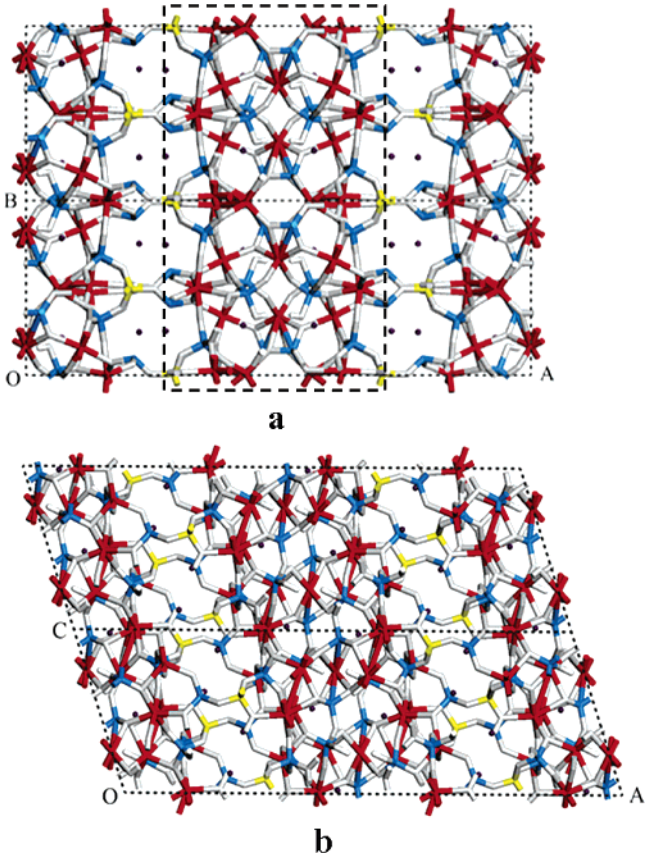

Figure 2. Open framework of MnBPO-CJ26 viewed along the [001] (a) and [010] (b) directions. The double layer (I) is labeled by a dotted framework. Key: Mn, red; P, blue; B, yellow; N, purple; O, gray.

and one P−O−Mn bond; P(3) and P(4) each make two P−μ_3-O−Mn(Mn) bonds, one P−O−Mn bond, and one P−O−B bond; P(5) makes one P−μ_3-O−Mn(Mn) bond, one P−O−Mn bond, and one P−O−B bond, leaving one terminal P−O(4)H group. Their P−O bond lengths are in the range of 1.498(3)−1.581(3) Å. The one unique B atom is tetrahedrally coordinated and shares three μ_2-O atoms with adjacent P atoms and one OH group with Mn(5) atom.

Figure 2a and 2b shows the framework of MnBPO-CJ26 viewed along the [001] and [010] directions, respectively. Unlike the reported manganese borophosphates,[18,19,21−23] the structure of MnBPO-CJ26 features anionic manganese-phosphate double layers, $[Mn_9(OH)_2(HPO_4)_4(PO_4)_6]^{10-}$ (I), which are made up from the linkages of MnO_5, MnO_6, PO_4, and HPO_4 polyhedra (Figure 2a: dashed framework). These layers are further connected by BO_4 groups forming the 3-D open framework with 2-D 8-MR channels along the [010] and [001] directions, respectively. The complex layer (I), as seen in Figure 3a, can be viewed as composed of another two anionic manganese-phosphate single layers $[Mn_4(OH)(HPO_4)_2(PO_4)_2]^{3-}$ (II) (Figure 3a: dashed framework, and Figure 3b), which are further connected by MnO_6 and PO_4 polyhedra. The layer (II) is built up from MnO_5, MnO_6, PO_4, and HPO_4 polyhedra, giving rise to 6-MR windows in which the protonated NH_3 molecules reside to compensate the negative charge of the anionic framework. When all phosphorus atoms are omitted in the layer (I), a Mn−O−Mn double layer (III) (Figure 4a), consisting of two Mn−O−Mn single layers (IV), appears (Figure 4a: dashed framework, and Figure 4b). Within the layer (IV), $Mn(1)O_5$ bipyramids and $Mn(2)O_6$ octahedra are connected by apex-sharing, forming the infinite chains, while $Mn(4)O_5$ trigonal bipyramids and $Mn(5)O_6$ octahedra are connected by edge-sharing and apex-sharing, alternately forming additional infinite chains. The two chains are further connected by the quasi-squares composed of $Mn(2)O_6$ and $Mn(5)O_6$ octahedra, resulting in the 10-MR windows. Layers (IV) are further connected by $Mn(3)O_6$ octahedra through sharing corners with $Mn(2)O_6$ octahedra and $Mn(4)O_5$ bipyramids to form the layer (III). It is noted that the Mn−O−Mn layer is rare not only in manganese borophosphate compounds but also in manganese phosphates. Only one example is observed in the manganese phosphate mineral $Mn_5(H_2O)_4[PO_3(OH)_2](PO_4)_2$.[30,31] The fact that all the manganese atoms connecting with each other by oxygen atoms in MnBPO-CJ26 implies the possible existence of magnetic interactions.

Magnetic Studies of MnBPO-CJ26. The ESR spectrum of the powdered sample measured at room temperature shows a broad isotropic signal $g = 1.996$.

The variable-temperature magnetic susceptibility of MnBPO-CJ26 measured on a powder crystalline sample in the field of 5000 Oe is shown in Figure 5. The molar magnetic susceptibility per Mn^{2+} above 100 K obeys the Curie-Weiss law ($\chi_m = C/(T - \theta)$) very well with a Weiss constant, $\theta = -51.2(5)$ K, and a Curie constant, $C = 4.404(3)$ cm^3 mol^{-1} K. The latter corresponds to one spin-only Mn(II) ions with $S = {}^5/_2$ and $g = 2.007$. The $\chi_m T$ versus T curve measured in the field of 5000 kOe is shown in Figure 6. The $\chi_m T$ first decreases continuously with the decrease of temperature and reaches a minimum of 1.104 cm^3 mol^{-1} K at 17 K. The decrease of $\chi_m T$ and the negative Weiss constant suggest a dominated antiferromagnetic interaction. On further cooling, however, the rapid increase in $\chi_m T$ and the field dependence of the susceptibility below 8.0 K indicates the onset of long range order with a spontaneous magnetization.[32] According to the above observation, this magnetic behavior should be either ferrimagnetic or canted antiferromagnetic, which will be discussed below. The second drop of $\chi_m T$ below 8.0 K may arise from the magnetic field saturation effect and/or antiferromagnetic interaction between the layers. The fact that the decrease of $\chi_m T$ below 8.0 K at higher magnetic field is more than that at lower magnetic field (inset of Figure 6) implies a magnetic field saturation effect. The critical temperature (T_c) is further determined as 8.0 K from the maximum of χ_m' and the emergence of χ_m'', where χ_m' and χ_m'' are the in-phase and out-of-phase alternating current (ac) susceptibilities at zero external magnetic field and a 2 Oe oscillating field frequency range of 1−999 Hz (Figure 7). The field dependence of the magnetization (0−50 kOe) was measured at 4.0 K. As seen in Figure 8, the shape of the $M(H)$ curve is typical of a canted antiferromagnet with a fast increase of the resulting magnetization at very low fields and a linear variation of $M(H)$ at $H > 1.2$ T.[33] The

(30) ICSD: Moore, P. B.; Araki, T. *Am. Mineral.* **1973**, *58*, 302.
(31) Sharma, C. V. K.; Chusuer, C. C.; Clérac, R.; Möller, T.; Dunbar, K. R.; Clearliele, A. *Inorg. Chem.* **2003**, *42*, 8300.
(32) Chippindale, A.; Gaslain, F. M.; Bond, A. D.; Powell, A. V. *J. Mater. Chem.* **2003**, *13*, 1950.

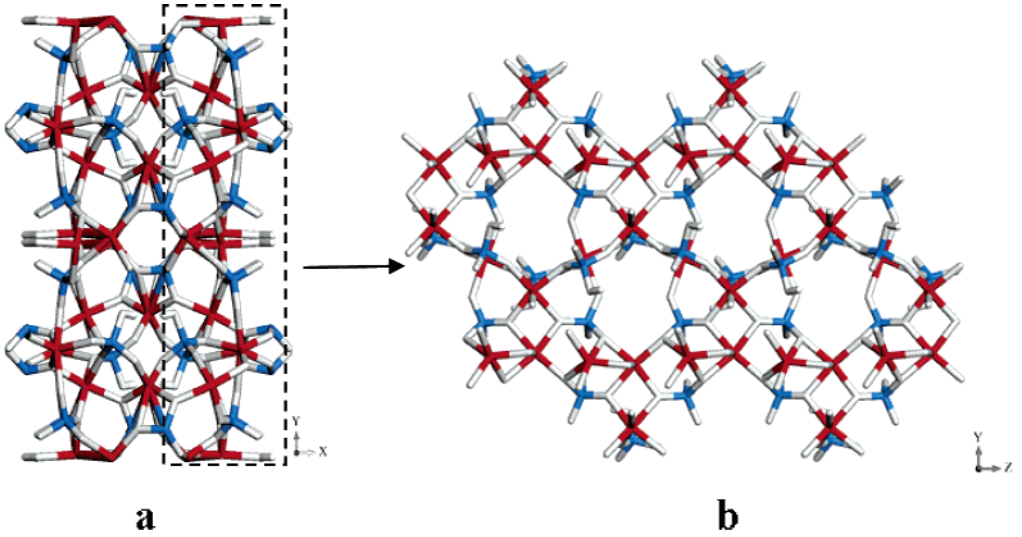

Figure 3. (a) The layer (I) viewed along the [001] direction. (b) The layer (II) viewed along the [100] direction. Key: Mn, red; P, blue; O, gray.

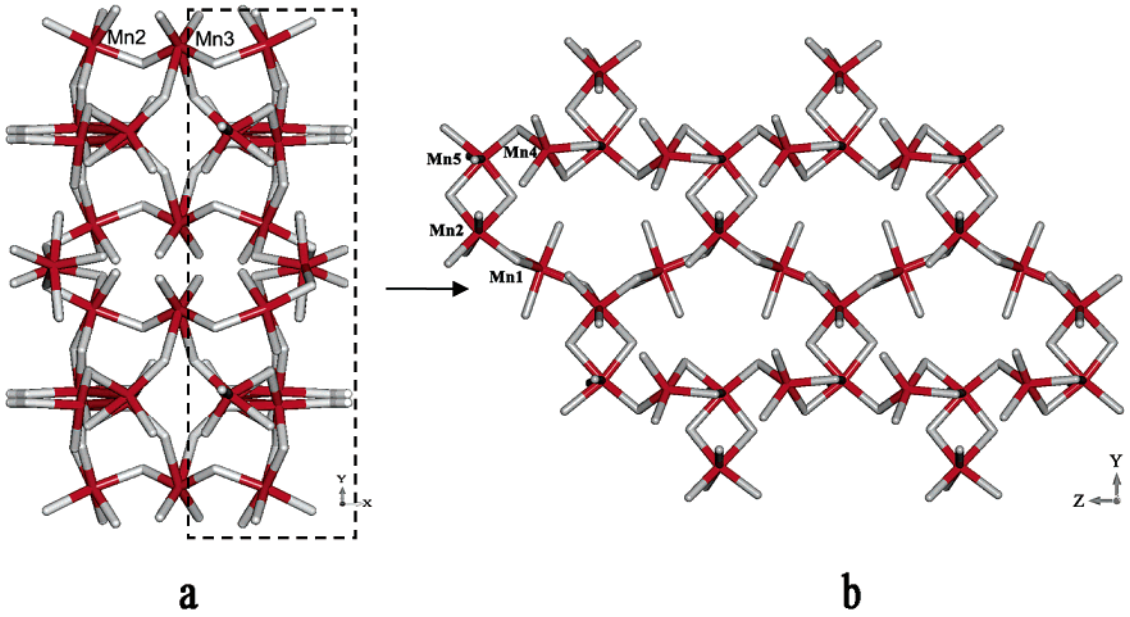

Figure 4. (a) The layer (III) viewed along the [001] direction. (b) The layer (IV) viewed along the [100] direction.

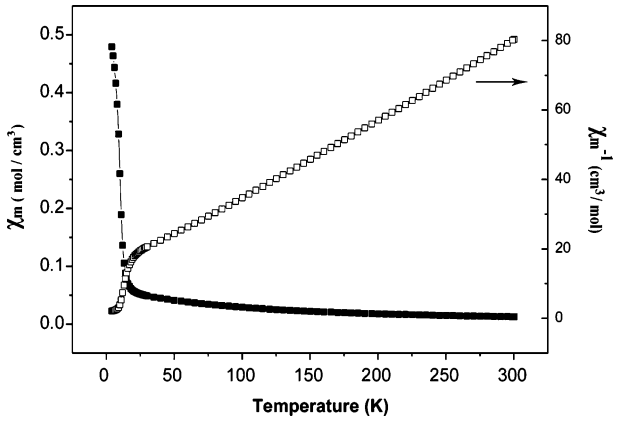

Figure 5. χ_m vs T and $1/\chi_m$ vs T plots with a measuring field of 5 kOe.

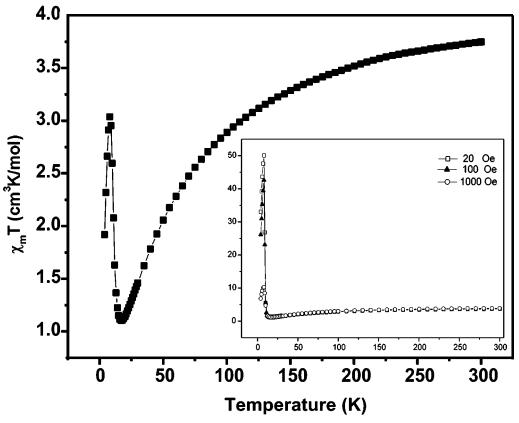

Figure 6. Temperature dependence of $\chi_m T$ measured with a field of 5 kOe. The inset is the temperature dependence of $\chi_m T$ measured with a field of 20, 100, and 1000 Oe, respectively.

curve reaches a value of 0.64 μ_B per Mn^{2+} ion which is considerably smaller than the value of 5 μ_B per Mn^{2+} ion expected for a ferromagnetically ordered phase. This lack of saturation at high fields further confirms that the low-

(33) Riou-Cavellec, M.; Lesaint, C.; Noguès, M.; Grenèche, J.; Férey, G. *Inorg. Chem.* **2003**, *42*, 5669.

(34) Carlin R. L. *Magnetochemistry*; Springer-Verlag: Berlin, 1986.

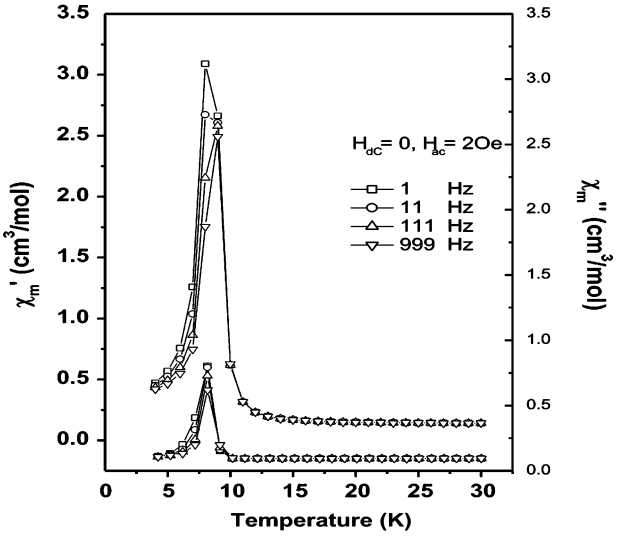

Figure 7. Zero-field *ac* susceptibility measurements performed in the range of 4−30 K, at H_{ac} = 2 Oe and frequencies of 1, 11, 111, and 999 Hz, showing both in-phase [$cM'(T)$] and out-of-phase [$cM''(T)$] signals at ca. 8.0 K.

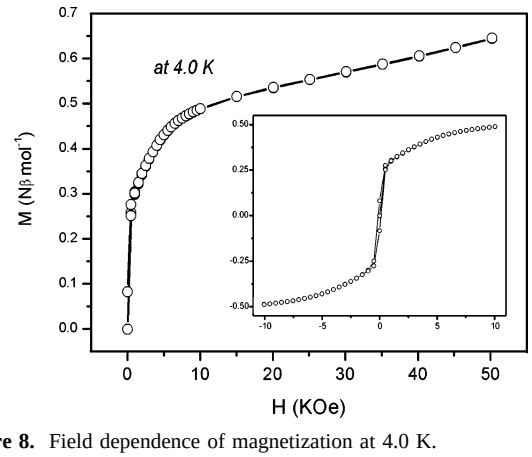

Figure 8. Field dependence of magnetization at 4.0 K.

temperature magnetic ground state is a canted antiferromagnet.[34−36]

Examination of the structure suggests that magnetic interactions between adjacent manganese-phosphate layers (I), which are ca. 6.578 Å apart (Mn···Mn) at a minimum, are likely to be comparatively weak. The Mn^{2+} ion is normally considered to be a Heisenberg spin and therefore magnetic order is only achieved once exchange interactions propagate in all three dimensions through the structure.[37] In this case, the exchange between bilayers is likely to be the limiting factor for long range order and reflected on a low value of T_c in relation to the Weiss constant. The stronger magnetic exchange might be dominated by intralayer interactions, predominately within those individual Mn−O−Mn double layers (III). Within the double layer (III), the MnO_5/MnO_6 polyhedra are connected by sharing common edges or common vertex with the Mn···Mn distances in the range of 3.144−4.094 Å. It is too large for significant direct magnetic exchange to occur, suggesting that coupling occurs via the oxygen anions. The possible superexchange pathways' cation−anion−cation angles and Mn−Mn distances are listed in Table 3. According to the qualitative coupling rules developed by Goodenough-Kanamori,[38] all these superexchange interactions which are between high-spin d^5 ions via anion p-orbitals will be antiferromagnetic. The presence of a ferromagnetic component and the small magnetization at high field are indicative of possible spin canting, resulting from the absence of an inversion center between the neighboring Mn ions.[39−41] In general, the complexity of the structure implies a very complicated magnetic behavior which prevents a simple explanation. Further investigation is undergoing.

Table 3. Mn−O−Mn Bond Angles (deg) and Distances (Å) for MnBPO-CJ26

	angles (deg)	distance (Å)
Mn1−O5−Mn2	108.25(11)	3.478
Mn1−O6−Mn2	110.36(11)	3.610
Mn2−O18−Mn5	100.36(9)	3.365
Mn2−O19−Mn5	96.80(9)	3.365
Mn4−O11−Mn5	90.41(9)	3.144
Mn4−O14−Mn5	91.19(9)	3.144
Mn4−O15−Mn5	107.00(10)	3.488
Mn2−O9−Mn3	121.23(12)	3.687
Mn4−O12−Mn3	123.87(11)	4.094

Conclusions

By using a hydrothermal synthesis method, a new open-framework manganese(II) borophosphate with unique B/P and Mn/P ratios (B/P = 1/5, Mn/P = 9/10) has been successfully prepared. The three-dimensional structure has 2-D 8-MR channels along the [010] and [001] directions. It is based on anionic manganese-phosphate double layers $[Mn_9(OH)_2(HPO_4)_4(PO_4)_6]^{10-}$, which are pillared by BO_4 tetrahedra. The complex anionic layers (I) can be described as built up from individual manganese-phosphate single layers (II), Mn−O−Mn double layers (III), and Mn−O−Mn single layers (IV). Magnetic measures reveal that this compound shows canted antiferromagnetism below 8.0 K. The infinite Mn−O−Mn layers are believed to be responsible for this behavior. The complex superexchange mechanism needs to be further investigated. The synthesis of this novel compound and finding of its magnetic property will promote further development of new open-framework materials with interesting physical properties.

Acknowledgment. This work is supported by the National Natural Science Foundation of China and the State Basic Research Project of China (G2000077507).

Supporting Information Available: The XRD pattern, IR spectrum, TG curve, crystallographic data (CIF), atomic coordinates with isotropic temperature factors and hydrogen bonds. This material is available free of charge via the Internet at http://pubs.acs.org.

CM052170M

(35) Merchant, S.; McElearney, J. N.; Shankle, G. E.; Carlin, R. L. *Physica* **1974**, *78*, 308.
(36) Sanz, F.; Parada, C.; Rojo, J. M.; Ruiz-Valero, C. *Chem. Mater.* **2001**, *13*, 1334.
(37) Mermin, N. D.; Wagner, H. *Phys. Rev. Lett.* **1966**, *17*, 1133.
(38) Goodenough, J. B. *Magnetism and the Chemical Bond*; Wiley: New York, 1963.
(39) Bellitto, C.; Federici, F.; Colapietro, M.; Portalone, G.; Caschera, D. *Inorg. Chem.* **2002**, *41*, 709.
(40) Moriya, T. *Phys. Rev.* **1960**, *117*, 635.
(41) Dzyaloshinsky, I. *J. Phys. Chem. Solids* **1958**, *4*, 241.